Polymer 51 (2010) 902–907

Contents lists available at ScienceDirect

Polymer

journal homepage: www.elsevier.com/locate/polymer

Hybrid nanocomposites of semiconductor nanoparticles and conjugated polyelectrolytes and their application as fluorescence biosensors

Zhen Gu [a,c], Xiao-Yuan Chen [b], Qun-Dong Shen [a,*], Hai-Xiong Ge [b], Hai-Hua Xu [b]

[a] Department of Polymer Science & Engineering and Key Laboratory of Mesoscopic Chemistry of MOE, School of Chemistry & Chemical Engineering, Nanjing University, Nanjing 210093, China
[b] Department of Material Science & Engineering and National Laboratory of Solid State Microstructures, Nanjing University, Nanjing 210093, China
[c] Department of Chemical and Biomolecular Engineering, Department of Mechanical and Aerospace Engineering, University of California, Los Angeles, CA 90095, USA

ARTICLE INFO

Article history:
Received 28 September 2009
Received in revised form
8 December 2009
Accepted 31 December 2009
Available online 11 January 2010

Keywords:
Conjugated polymers
Fluorescence
Biosensors

ABSTRACT

Weakly emissive silicon nanoparticles with an average diameter of about 5 nm are prepared via pulsed laser ablation of silicon wafers in water. Electrostatic assembly of water-soluble conjugated polyelectrolytes on the surface of the silicon nanoparticles steadily enhances the photoluminescence of these nanocomposites, indicating the possibility of energy transfer between the semiconductor nanoparticles and the conjugated polymer, or silicon nanoparticle-induced elimination of chain aggregates of the conjugated polyelectrolyte. Fluorescence emission of the hybrid silicon-conjugated polymer nanocomposites is steeply quenched by cytochrome *c*, and the minimum detection concentration for the redox-active protein is found to be 50 nM. The sensitization is realized by ultrafast photoinduced electron transfer between the electron-deficient protein and the conjugated polyelectrolyte binding on the silicon nanoparticle surfaces. The results offer guidelines to explore novel sensors for detecting nanoparticles, and also help develop high-efficiency sensory materials based on electrostatic complexes of conjugated polyelectrolytes and inorganic semiconductor nanoparticles.

© 2010 Elsevier Ltd. All rights reserved.

1. Introduction

Semiconductor nanomaterials offer unique opportunities to study materials in the regime between molecular and bulk states due to the quantum confinement effect imposed upon their charge carriers [1]. Silicon plays a key role in mesoscopic semiconductor electronics. As an indirect band material, silicon is an inefficient emitter but shows dramatic changes in optical properties when its size is reduced to less than 10 nm. Recent investigations on silicon nanocrystals and one-dimensional silicon quantum wires show dramatic changes in their light-emission behavior [2,3]. The potential applications of silicon nanomaterials in optoelectronic devices, fluorescent labels for biological cell imaging, highly sensitive biological and chemical sensors, and non-volatile memory devices have triggered broad interests [4–9]. Silicon nanomaterials have been fabricated by electrochemical etching of silicon wafers, laser pyrolysis, high-temperature aerosol reactions, plasma deposition, and chemical reduction techniques in colloids or microemulsions [10–14]. To meet the requirements of biosensor applications, silicon nanoparticles should be water-dispersible, highly luminescent, and have functional groups for conjugation with biological molecules in aqueous environments.

The photoluminescence in the visible region renders the silicon nanoparticles potential fluorescent probes in biological systems. However, post-synthesis procedures for semiconductive nanomaterials are generally required to afford a substantial photoluminescence quantum yield and hydrophilicity to prevent aggregation and precipitation in a biological environment. For example, the silicon nanoparticles have been chemically modified with allylamine by a platinum-catalyzed addition reaction to hydrogen-terminated surfaces [15]. In comparison with these chemical processes, we describe a rather simple method by electrostatic adsorption of oppositely charged conjugated polyelectrolytes on the silicon nanoparticle surfaces. The chemical structure of the polyelectrolyte, poly[(2-methoxy-5-propyloxy sulfonate-1,4-phenylene vinylene)-alt-(1,4-phenylene vinylene)], is shown in Fig. 1. The water-soluble polyelectrolyte has a π-conjugated backbone, which can be regarded as an array of charged chromophores (or fluorophores) that are fully conjugated [16,17]. Thus it can absorb/emit light that is consistent with its band gap, and most importantly, effectively transport electrons or energy along the "molecular wire" of chromophores [18–23]. Electrostatic assembly thereby affords dual-fluorescent composite nanoparticles with inorganic semiconductor cores and shells of ultrathin organic

* Corresponding author. Tel.: +86 25 83317807; fax: +86 25 83317761.
E-mail address: qdshen@nju.edu.cn (Q.-D. Shen).

0032-3861/$ – see front matter © 2010 Elsevier Ltd. All rights reserved.
doi:10.1016/j.polymer.2009.12.035

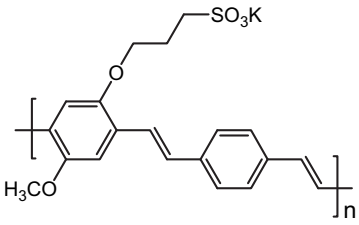

Fig. 1. Chemical structure of an anionic conjugated polyelectrolyte described in this study.

semiconductor layers. This hybrid nanocomposites can serve as a high-sensitivity fluorescence sensor for the detection of the redox-active metalloprotein cytochrome *c*.

2. Experimental section

2.1. Materials

The conjugated polyelectrolyte was obtained by the Wittig condensation reaction [24,25], and the number- and weight-average molecular weights of it are 12,100 Da and 19,800 Da, respectively. Horse heart cytochrome *c* (molecular mass 12,384 Da) from Sigma and cetyltrimethylammonium bromide (CTAB) from Shanghai Chemical Reagent Company were used as received. Silicon wafers were obtained from Huajing Microelectronics (Wuxi, China). The water used in making the stock solution of the conjugated polyelectrolyte, cytochrome *c*, and CTAB was purged with nitrogen gas for at least 2 h immediately prior to usage.

2.2. Preparation of water-dispersible silicon nanoparticles [26]

A silicon wafer was positioned in a beaker filled with de-ionized water and 2.3 mM of CTAB. The target was irradiated by KrF laser pulses (248 nm in wavelength, 25 ns in pulse width and 5 Hz in repetition rate, with a laser fluence of ~2 J/cm^2) equipped with controlled laser fluences and pulse numbers.

2.3. Instrumentation and measurements

The silicon content in the nanoparticles was determined by inductively coupled plasma-atomic emission spectrometry (JA1100, Jarrell–Ash Apparatus, USA) using a standard protocol for the silicon sample treatment. The emission spectra were measured on an SLM 48000 DSCF luminescence spectrometer. The excitation wavelength was chosen to coincide with the maximum absorption of electron spectrum measured by a Shimadzu UV-3100 spectrophotometer. The morphology of the silicon nanoparticles was observed by a transmission electron microscope (Philips Tecnai F20 S-Twin with field emitter). Samples for the microstructure observation were prepared by adding drops of aqueous solution of the silicon nanoparticles on electron microscope grids and then dried.

3. Results and discussion

3.1. Photophysical properties of hybrid nanocomposites

Herein, the silicon nanoparticles are prepared by pulsed laser ablation (PLA) [26,27] of silicon wafer in aqueous solution containing cationic surfactant of CTAB (2.3 mM). The as-prepared nanoparticles have an average diameter of about 5 nm observed by a transmission electron microscope (Fig. 2a). The result of inductively coupled plasma-atomic emission spectroscopy indicates that the silicon nanoparticles are at a concentration of 2.0 μg/mL. The photoluminescence spectrum (Fig. 2b) shows that the silicon nanoparticles in aqueous solution are weakly blue-emissive with an emission peak at 457 nm and a full-width at half maximum height of 60–70 nm. The asymmetric broad profile of the emission spectrum is attributed to a large size distribution of the silicon nanoparticles prepared by PLA. The band gap of the silicon nanoparticles is enlarged with respect to bulk silicon due to a quantum confinement effect, which in turn increases the probability of radiative recombination through the direct band gap transitions and reduces phonon-assisted indirect band gap transitions.

A layer of the conjugated polyelectrolyte is assembled on the silicon nanoparticles by the following procedure. In brief, the conjugated polyelectrolyte with weight-average molecular weight of 19,800 Da is readily dissolved in water to make a 10 μM (based on the repeat unit) solution, and then 20 μM surfactant CTAB is added. Complexation of the polyelectrolyte with the charged silicon nanoparticles is performed by gradually adding the silicon nanoparticle stock solution into the solution of the conjugated polyelectrolyte. The aqueous mixture is then stirred to ensure the completion of electrostatic adsorption. A sequence of fluorescence emission spectra were taken for each step of addition of the nanoparticles. Emission intensity and peak position as a function of

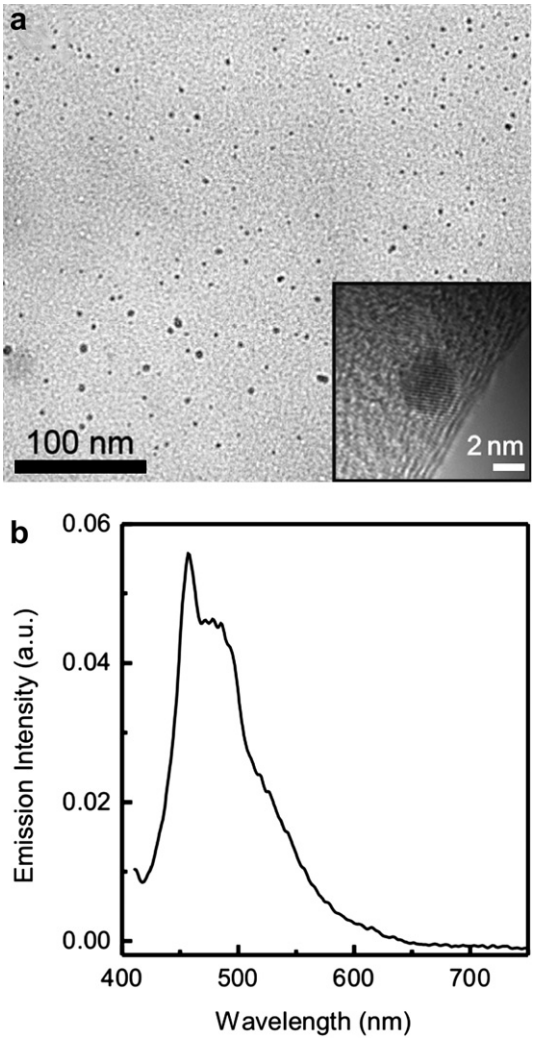

Fig. 2. (a) TEM image of the silicon nanoparticles on a carbon grid. Insert: a high resolution TEM image of an individual silicon nanoparticle. (b) Photoluminescence spectrum of the silicon nanoparticles in an aqueous CTAB solution. The excitation wavelength was 390 nm.

silicon nanoparticle contents are shown in Fig. 3. Continuous emission enhancement and a blue-shift of the fluorescence peak indicate that electrostatic assembly of the conjugated polyelectrolytes and silicon nanoparticles occurs.

It is important to elucidate the fundamental processes correlated with photophysical properties of the current system. Immediately after mixing 33.3 ng/mL (final concentration) silicon nanoparticles with the solution, emission intensity increases to a value obviously larger than that of the parent liquids (Fig. 4a). As-prepared silicon nanoparticles are stabilized by capping ligands from small molecule-weight surfactants. The conjugated polyelectrolyte has a large number of ionic groups and aromatic rings, which enable a strong adsorption at the silicon nanoparticle surfaces by electrostatic and hydrophobic interactions. Upon formation of a layer of the conjugated polyelectrolyte on the silicon nanoparticles, intrinsic emission of the polymer is clearly observed. The spectral shape is nearly identical to that of the conjugated polyelectrolyte and only a slight blue-shift (6 nm) of the emission maximum is observed. One may also anticipate detecting emission from silicon nanoparticles, which can also be excited by 395 nm ultraviolet light. However, the emission around 457 nm can hardly be seen, indicating the silicon nanoparticles cannot be solely responsible for the fluorescence enhancement of the solution. Thereby, the enhancement should be relevant to the interactions between the conjugated polymers and the nanoparticles in the ground or excited states. It has been reported that blends of semiconductor nanocrystals and conjugated polymers exhibit resonance energy transfer (RET) [28–32], where an excited chromophore (the donor) can transfer energy to another chromophore (the acceptor) and induce emission of the latter [33]. The emission enhancement can therefore be attributed to the energy transfer from the optically excited silicon nanoparticles (core) to the wrapped conjugated polyelectrolyte chains (shell) in the excited complex.

By increasing the final concentration of silicon nanoparticles to 66.7 ng/mL, emission intensity at spectral position of the conjugated polyelectrolyte increases (Fig. 4a). Both changes in the spectral shape and significant blue-shift of peak position to 495 nm are discernable. At the same time, there is a fast emission intensity increase of the newly formed peak with further introduction of the silicon nanoparticles (Fig. 4b). The results indicate another mechanism associated with the fluorescence enhancement, i.e. silicon nanoparticle-induced elimination of chain aggregates of the conjugated polyelectrolyte, which has a hydrophobic water-insoluble backbone. Thereby the amphiphilic polyelectrolyte has a strong tendency to aggregate, i.e. self-assemble in aqueous media through hydrophobic interactions. As shown in Fig. 4c, the formation of aggregate species of the conjugated polyelectrolyte is more evident in fluorescence spectra recorded in aqueous solution with surfactant, where the maximum emission wavelength is nearly the same as that in solid-state film. Meanwhile, break-up of the aggregated conjugated polyelectrolyte chains in an aqueous solution containing 90 volume percent of methanol is associated with a large blue-shift of emission peak.

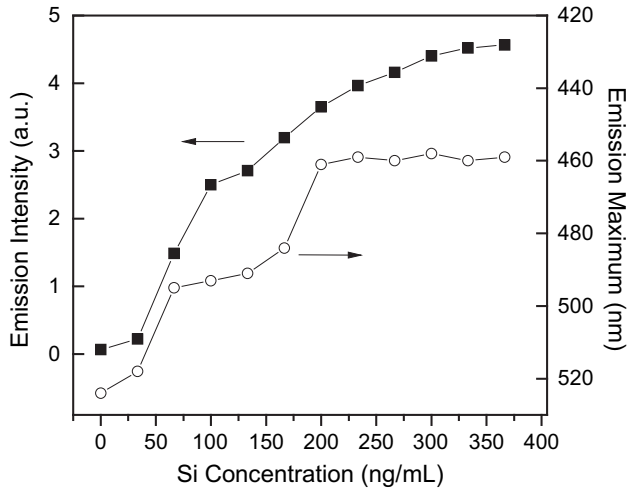

Fig. 3. Dependence of fluorescence emission intensity (monitored at 458 nm; solid square, left-hand *y*-axis) and peak position (open circle, right-hand *y*-axis) on the silicon nanoparticle feeding levels.

When the nanoparticle levels are higher than 200 ng/mL, a well-defined peak at 458 nm becomes dominative in the photoluminescence spectrum and remains unchanged irrespective of the nanoparticle incorporation (Fig. 4b), suggesting a saturated adsorption of the conjugated polyelectrolyte layer. In comparison, the aggregate-free conjugated polyelectrolyte has an emission maximum at 475 nm. The conjugated polyelectrolyte chains totally wrap around the nanoparticle. The blue-shift may arise from bending of the conjugated backbones on surfaces with nanoscopic curvature. However, a decrease of fluorescence quantum yield should also be expected when effective conjugation lengths of the chain backbones are shortened, which is contradictory to the observation of emission enhancement. On the other hand, the conjugated polyelectrolyte chains behave as rigid rods. Decrease in coplanarity of the conjugated backbone, if any, is unlikely to result in such a large blue-shift (17 nm). Therefore the shortest-wavelength peak at saturation adsorption most likely originates from the silicon nanoparticles. Full control over surface properties of semiconductor nanoparticles is particularly important to achieve desirable emission characteristics. The emission intensity of silicon nanoparticles is reported to be dependent on its degree of surface passivation [34]. Encapsulation of the silicon nanoparticles by hydrophobic conjugated chains may eliminate surface traps and improve fluorescence emission efficiency of the former.

3.2. Hybrid nanocomposites for cytochrome c detection

The assembly of molecular layers on nanoparticle surfaces plays an important role in their functionalization. Luminescent semiconductor nanoparticles with modified surfaces have been extensively used to detect biological molecules and in cellular imaging [35,36]. The silicon nanoparticles encapsulated by the conjugated polyelectrolytes have a high surface density of ionic moieties and simultaneously high fluorescence yield, thus they can serve as an ideal probe for biological molecules. Cytochrome *c*, a highly soluble and redox-active protein involved in biological electron transfer processes, is subsequently investigated. By the in situ fluorescence method, the minimum detection concentration for the cytochrome *c* is found to be 50 nM, where the addition of the protein results in fluorescence quenching of the nanocomposites of silicon nanoparticles and conjugated polyelectrolytes (Fig. 5). Cytochrome *c* at a concentration lower than 600 nM can suppress emission from the composite nanoparticles to one-half of their original intensity.

The quenching process can be quantitatively described by the Stern–Volmer equation:

$$\frac{PL_0}{PL} = 1 + K_{SV}[Q] \quad (1)$$

where PL_0 and PL are the steady-state emission intensities monitored at 458 nm in the absence and in the presence of quencher (concentration of which: [*Q*]), respectively. The Stern–Volmer constant (K_{SV}) provides a direct measurement of the quenching efficiency or sensitivity. At protein concentrations ranging from 0 to

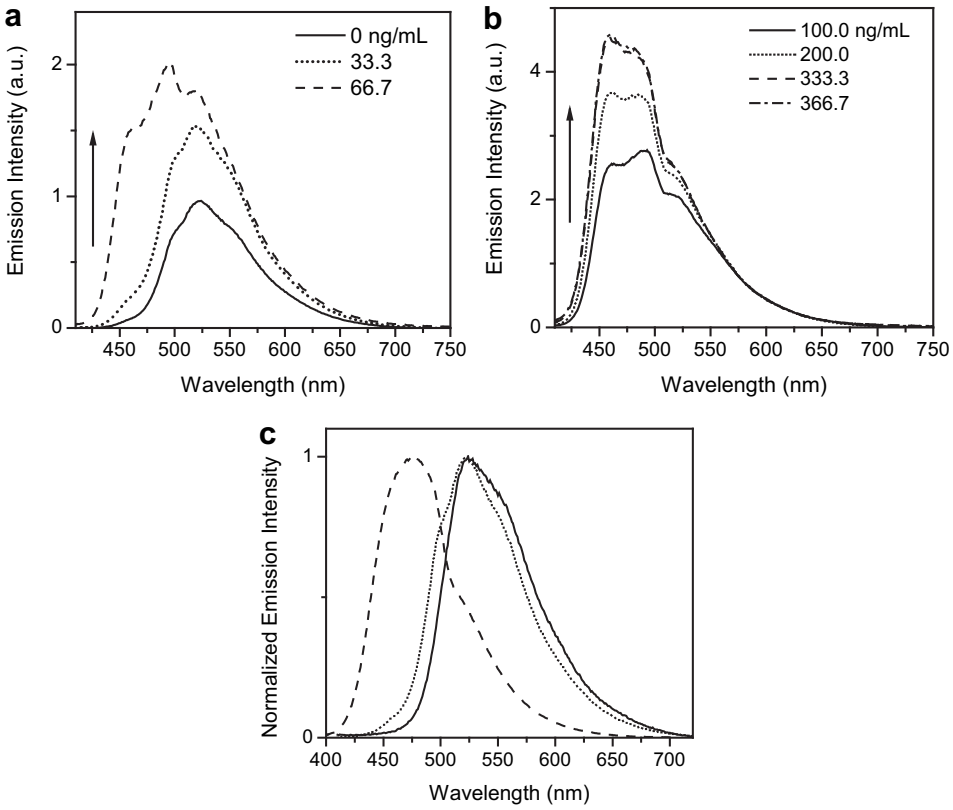

Fig. 4. (a, b) Photoluminescence spectra of the conjugated polyelectrolyte alone (0 ng/mL) and its electrostatic assemblies with the silicon nanoparticles (33.3–366.7 ng/mL). Arrows indicate the direction of change in emission intensity with continuous addition of the nanoparticles. The excitation wavelength is 395 nm. (c) Emission spectra of the conjugated polyelectrolyte in a solid-sate film (solid line), in aqueous solution with 20 μM surfactant (dotted line), and in a mixed solvent (9/1 v/v) of methanol and water (dashed line).

450 nM, a linear plot with K_{SV} of 1.5 × 10^6 $mol^{-1}L$ is obtained (Fig. 6). The quenching efficiency is pronounced if one considers a fluorescence quenching system of small molecule-weight stilbene (the fluorophore) and methylviologen (the quencher) whose K_{SV} is as low as 15.3 $mol^{-1}L$ [37]. Such high-sensitivity is also notable among recently reported results using conducting polyelectrolytes for protein detections [38–40]. To elucidate the mechanisms operating in the case of cytochrome *c* quenching of the composite nanoparticle fluorescence, a control experiment is conducted to explore whether the fluorescence of individual components of the composite nanoparticles are influenced by the protein. Upon incubation of the conjugated polyelectrolyte with the stock solution of cytochrome *c*, fluorescence quenching is also observed (Fig. 6).

Cytochrome *c* consists of a single heme (iron-containing porphyrin) group and its heme iron is ligated to two amino acid side chains. Both ferric and ferrous redox states are physiologically relevant. Therefore the protein is capable of undergoing oxidation and reduction. The Horse heart cytochrome *c* as-received is predominantly in the oxidized form, making it an efficient electron acceptor. In the oxidized state, the protein is also locally unfolded, thereby enhances exposure of the heme group to water [41] and ensures easy access of the conjugated polymer through electrostatic or hydrophobic interactions. On the other hand, the conjugated polyelectrolyte can absorb photons and the optical excitations generate bound excitons (electron–hole pairs) or free electronic carriers which migrate independently throughout the molecular wires. When the electrons move to trapping sites of cytochrome *c*, a fast electron transfer from the excited state of the conjugated polyelectrolytes to the oxidized ferric state of the protein occurs. In such photoinduced electron transfer processes, the energy required to re-emit as fluorescence from the conjugated polymer is diminished as chemical energy, and thereby fluorescence quenching occurs. An alternative fluorescence quenching process is resonance energy transfer from the conjugated polyelectrolytes (donor) to the heme groups (acceptor),

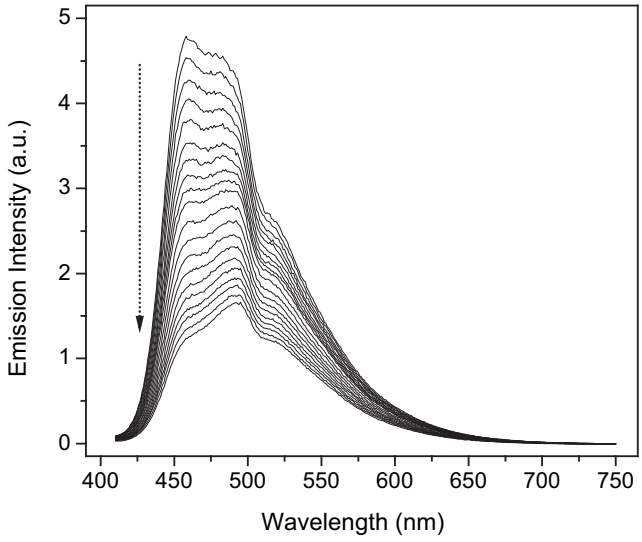

Fig. 5. Influence of cytochrome *c* (from 0 to 950 nM with concentration increments of 50 nM) on the fluorescence spectra of dual-fluorescent nanocomposite of the silicon nanoparticles and conjugated polyelectrolytes. The excitation wavelength is 395 nm. The arrow indicates the direction of change in emission intensity with increasing concentration of cytochrome *c*.

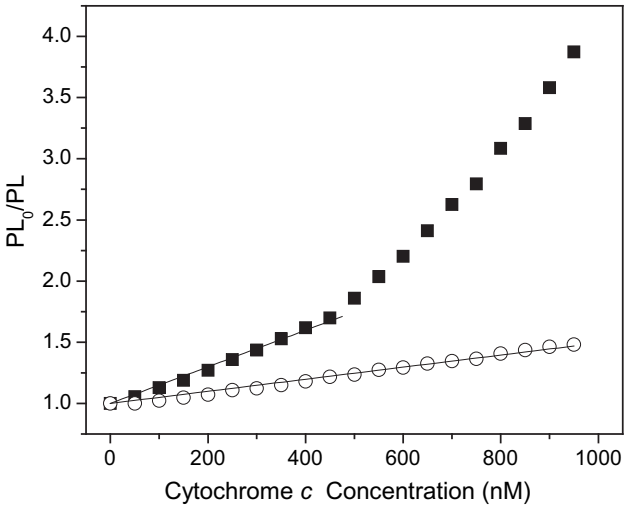

Fig. 6. Stern–Volmer quenching plots for the composite nanoparticles (solid square) and the conjugated polyelectrolyte alone (open circle). Solid curves are best fitted by Equation (1).

which is excluded since no obvious enhancement in the emission at longer wavelength can be found. The extremely large quenching efficiency in the current system can be readily attributed to 1) "concentration enhancement" effect, i.e. facile binding of positively charged cytochrome *c* (pI: 10.0–10.5) [42] to the negatively charged conjugated polymer chains. 2) The "molecular wire" effect, i.e. rapid and highly efficient transport of the electronic excited states to the quencher sites plays another important role in high sensitive response of the composite nanoparticles or the conjugated polyelectrolytes [43,44]. In contrast, our recent study reveal that non-metalloprotein bovine serum albumin (BSA, pI: 4.8, 66.3 kDa) and metalloprotein haemoglobin (pI: 7.0, 64 kDa) have insignificant quenching effects on composite nanoparticles that proteins with a final concentration of 1 μM can only suppress ~ 5% original emission intensity of nanocomposites. In addition to the redox activity of proteins, the distinct quenching efficiency can also result from the physical hallmarks of proteins, including surface charge, hydrophobic property and even molecular weight. A systematic study is under investigation.

Until now, the effect of the nanoparticles on the conjugated polyelectrolytes has not been fully appreciated. The conjugated polyelectrolyte alone has significantly inferior fluorescence quenching efficiency ($K_{SV} = 0.5 \times 10^6$), about one third of the value of the composite nanoparticles (Fig. 6). Another noticeable difference is that two concentration regions (0–450 nM and 500–1000 nM) having a linear Stern–Volmer relationship but different quenching constants are found for evolution of the composite nanoparticle fluorescence with the protein concentration. In contrast there exists a linear response of conjugated polyelectrolytes over the entire concentration range of cytochrome *c*. Electron transfer depends, to a large extent, on the life-time of excitation states and diffusion rate of the carriers towards the quencher binding site. Energy transfer from the excited silicon nanoparticles to the conjugated polyelectrolytes greatly attenuates the exciton population, and thereby the emission intensity and life-time of the conjugated polymer. Meanwhile, electrostatic assembly effectively eliminates the aggregation of the conjugated polyelectrolyte chains in aqueous media, thereby reducing the amount of the weakly emissive interchain species with short life-time and increases the diffusion length of the excitons [45]. Such effects may be responsible for improved sensitivity gains in the conjugated polyelectrolytes encapsulated on the silicon nanoparticles.

4. Conclusion

Water-dispersible silicon nanoparticles can readily take up conjugated polyelectrolytes by electrostatic assembly to afford dual-fluorescent composite nanoparticles with inorganic semiconductor cores and shells of ultrathin organic semiconductor layer. Such inorganic-organic hybrid semiconductors have high surface density of ionic moieties and simultaneous high fluorescence yield and can be exploited to develop sensors for trace analysis of biological molecules. The nanocomposites are highly sensitive to cytochrome *c*. The sensitization is realized by ultrafast photoinduced electron transfer between the electron-deficient protein and the conjugated polyelectrolytes binding on the silicon nanoparticle surfaces. The robust properties of the hybrid structure, convenient preparation and high-sensitivity merit, coupled with modern microscopy techniques and advanced nanobiotechnology [46–48], render this sensory material as a promising fashion for biomolecular detection and biomedical diagnostics.

Acknowledgement

This work is supported by the National Natural Science Foundation of China under Contract No. 20774040.

References

[1] Alivisatos AP. Science 1996;271:933–7.
[2] Chao Y, Siller L, Krishnamurthy S, Coxon PR, Bangert U, Gass M, et al. Nat Nanotechnol 2007;2:486–9.
[3] Holmes JD, Johnston KP, Doty RC, Korgel BA. Science 2000;287:1471–3.
[4] Hirschman KD, Tsybeskov L, Duttagupta SP, Fauchet PM. Nature 1996;384:338–41.
[5] Pavesi L, Dal Negro L, Mazzoleni C, Franzo G, Priolo F. Nature 2000;408:440–4.
[6] Li ZF, Ruckenstein E. Nano Lett 2004;4:1463-–7.
[7] Cui Y, Wei QQ, Park HK, Lieber CM. Science 2001;293:1289–92.
[8] Li Z, Chen Y, Li X, Kamins TI, Nauka K, Williams RS. Nano Lett 2004;4:245–7.
[9] Tiwari S, Rana F, Hanafi H, Hartstein A, Crabbe EF, Chan K. Appl Phys Lett 1996;68:1377–9.
[10] Wang L, Reipa V, Blasic J. Bioconjug Chem 2004;15:409–12.
[11] Li XG, He YQ, Talukdar SS, Swihart MT. Langmuir 2003;19:8490–6.
[12] Littau KA, Szajowski PJ, Muller AJ, Kortan AR, Brus LE. J Phys Chem 1993;97:1224–30.
[13] Takagi H, Ogawa H, Yamazaki Y, Ishizaki A, Nakagiri T. Appl Phys Lett 1990;56:2379–80.
[14] Tilley RD, Warner JH, Yamamoto K, Matsui I, Fujimori H. Chem Commun; 2005:1833–5.
[15] Warner JH, Hoshino A, Yamamoto K, Tilley RD. Angew Chem Int Ed 2005;44:4550–4.
[16] Jiang H, Taranekar P, Reynolds JR, Schanze KS. Angew Chem Int Ed 2009;48:4300–16.
[17] Thomas SW, Joly GD, Swager TM. Chem Rev 2007;107:1339–86.
[18] Huang X, Xu Y, Zheng L, Meng J, Cheng Y. Polymer 2009;50:5996–6000.
[19] Wang W, Wang R, Zhang C, Lu S, Liu T. Polymer 2009;50:1236–45.
[20] Xing C, Shi Z, Yu M, Wang S. Polymer 2008;49:2698–703.
[21] Li Y, Zhang W, Li G, Ju Y. Polymer 2008;49:225–33.
[22] O'Connell MJ, Chan CK, Li W, Hicks RK, Doorn SK, Wang HL. Polymer 2007;48:7582–9.
[23] Liu Y, Zong L, Zheng L, Wu L, Cheng Y. Polymer 2007;48:6799–807.
[24] Gu Z, Bao YJ, Zhang Y, Wang M, Shen QD. Macromolecules 2006;39: 3125–31.
[25] Gu Z, Shen QD, Zhang J, Yang CZ, Bao YJ. J Appl Polym Sci 2006;100: 2930–6.
[26] Chen XY, Lin J, Liu JM, Liu ZG. Appl Phys A 2009;94:649–56.
[27] Simakin AV, Voronov VV, Kirichenko NA, Shafeev GA. Appl Phys A 2004;79:1127–32.
[28] Kaufmann S, Stoferle T, Moll N, Mahrt RF, Scherf U, Tsami A, et al. Appl Phys Lett 2007;90:071108.
[29] Lutich AA, Jiang G, Susha AS, Rogach AL, Stefani FD, Feldmann J. Nano Lett 2009;9:2636–40.
[30] Chang TWF, Musikhin S, Bakueva L, Levina L, Hines MA, Cyr PW, et al. Appl Phys Lett 2004;84:4295–7.
[31] Anni M, Manna L, Cingolani R, Valerini D, Creti A, Lomascolo M. Appl Phys Lett 2004;85:4169–71.
[32] Stoferle T, Scherf U, Mahrt RF. Nano Lett 2009;9:453–6.
[33] Medintz IL, Clapp AR, Mattoussi H, Goldman ER, Fisher B, Mauro JM. Nat Mater 2003;2:630–8.
[34] Seraphin AA, Ngiam ST, Kolenbrander KD. J Appl Phys 1996;80:6429–33.

[35] Chan WCW, Nie SM. Science 1998;281:2016–8.
[36] Medintz IL, Uyeda HT, Goldman ER, Mattoussi H. Nat Mater 2005;4:435–46.
[37] Chen LH, McBranch DW, Wang HL, Helgeson R, Wudl F, Whitten DG. Proc Natl Acad Sci U.S.A 1999;96:12287–92.
[38] Sandanaraj BS, Demont R, Aathimanikandan SV, Savariar EN, Thayumanavan S. J Am Chem Soc 2006;128:10686–7.
[39] You CC, Miranda OR, Gider B, Ghosh PS, Kim IB, Erdogan B, et al. Nat Nanotechnol 2007;2:318–23.
[40] Wang J, Liu B. Chem Commun 2009;17:2284–6.
[41] Sagle LB, Zimmermann J, Matsuda S, Dawson PE, Romesberg FE. J Am Chem Soc 2006;128:7909–15.
[42] Van Gelder BF, Slater EC. Biochim Biophys Acta 1962;58:593–5.
[43] Zhou Q, Swager TM. J Am Chem Soc 1995;117:12593–602.
[44] Fan CH, Plaxco KW, Heeger AJ. J Am Chem Soc 2002;124:5642–3.
[45] Nguyen TQ, Doan V, Schwartz BJ. J Chem Phys 1999;110:4068–78.
[46] Huang B, Bates M, Zhuang XW. Annu Rev Biochem 2009;78:993–1016.
[47] Salaita K, Wang YH, Mirkin CA. Nat Nanotechnol 2007;2:145–55.
[48] Gu Z, Huang SX, Chen Y. Angew Chem Int Ed 2009;48:952–5.